Hindawi
International Journal of Aerospace Engineering
Volume 2017, Article ID 1823056, 17 pages
https://doi.org/10.1155/2017/1823056

Research Article

Characterization of the Aerodynamic Ground Effect and Its Influence in Multirotor Control

Pedro Sanchez-Cuevas, Guillermo Heredia, and Anibal Ollero

Robotics, Vision and Control Group, University of Seville, Seville, Spain

Correspondence should be addressed to Guillermo Heredia; guiller@us.es

Received 14 February 2017; Revised 6 July 2017; Accepted 13 July 2017; Published 17 August 2017

Academic Editor: Kenneth M. Sobel

This paper analyzes the *ground effect* in multirotors, that is, the change in the thrust generated by the rotors when flying close to the ground due to the interaction of the rotor airflow with the ground surface. This effect is well known in single-rotor helicopters but has been assumed erroneously to be similar for multirotors in many cases in the literature. In this paper, the ground effect for multirotors is characterized with experimental tests in several cases and the *partial ground effect*, a situation in which one or some of the rotors of the multirotor (but not all) are under the ground effect, is also characterized. The influence of the different cases of ground effect in multirotor control is then studied with several control approaches in simulation and validated with experiments in a test bench and with outdoor flights.

1. Introduction

In the last years, there has been a growing interest in Unmanned Aerial Vehicles (UAVs) [1]. UAVs of different sizes have been used in applications such as exploration, detection, precise localization, monitoring, and measuring the evolution of natural disasters. However, in most of these applications, the aerial robots are mainly considered as platforms for environment sensing. Then, the aerial robots do not modify the state of the environment and there are no physical interactions between the UAV and the environment. Furthermore, the interactions between the UAVs themselves are essentially information exchanges, without physical couplings between them.

Recently, the development of autonomous aerial robots with integrated robotic manipulators is catching much interest in robotic research [2, 3]. These *aerial manipulators* [4–6], as they are usually known, extend the range of possible applications of UAVs. For instance, aerial manipulators can be used for the inspection and maintenance of industrial plants and infrastructures [7], aerial power lines, and moving objects [8] and taking samples of material from areas that are difficult to access.

Aerial robotic manipulation with multirotors usually involves flying near objects, structures, and other obstacles, for example, to grasp or manipulate objects that are on the ground, over surfaces, near walls, or even under a surface. In all these cases, the multirotors will operate in hover or low speed near these horizontal or vertical surfaces. This paper studies the control of multirotor platforms under the influence of close ground surfaces on multirotors rotor thrust. Thus, for example, in the AEROARMS European project [9], aerial manipulators with multiple arms are used for inspection and maintenance in industrial settings and flying close to horizontal surfaces, and in the ARCAS European project [10], aerial robotic manipulation for assembly over a surface is considered (see Figure 1).

The wake of a rotorcraft can be greatly affected when the rotor is close to obstacles that disturb its free development. The most common of these effects is the one produced by the ground surface. This phenomenon, usually known as *ground effect*, is more pronounced in rotorcraft operating in hover and low speed. For rotorcraft hovering close to the ground, the rotor wake must rapidly expand as it approaches the surface, transitioning from the almost vertical downwash to radial outwash parallel to the ground. This alters the velocity

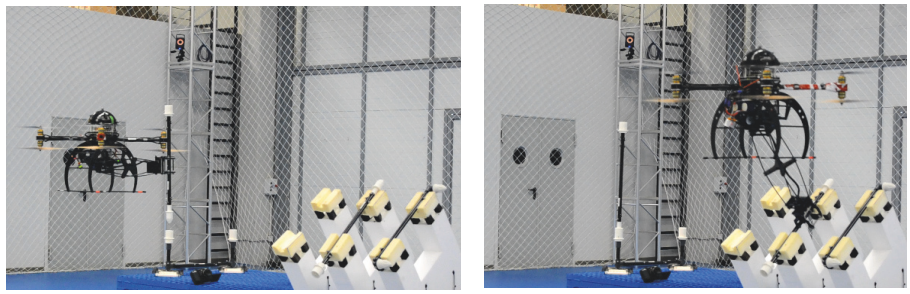

Figure 1: Structure assembly in the ARCAS project.

of the slipstream and the induced velocity, which then affects the rotor thrust and power. The ground effect in helicopters has been well researched in literature [11, 12] and has been studied for take-off, landing, and hovering near the ground [13–15]. However, for multirotors, it has not received much attention yet, although these platforms are being increasingly used in multiple applications.

The influence of ground effect in helicopters has been studied through the use of an underlying aerodynamic model or empirically. A classical analytical model for the ground effect is provided by [11], using potential flow with a single source to model the rotor airflow and the method of images to account for the ground effect. Other authors have provided empirical expressions for the rotor thrust increment in ground effect for large [16] and small UAV helicopters [17]. The model in [11] has been widely used because it has a simple analytical form and has been experimentally shown to accurately capture the relationship between rotor thrust in ground effect and rotor height over the ground surface.

The ground effect in multirotors has received much less attention. Several papers deal with the aerodynamic models of multirotors [18], which are used for navigation [19] or even for power control [20]. Disturbance observers have become popular in the last years for estimating external wrench in multirotors [21, 22]. In most cases, it is assumed that the external disturbance source is unique, mainly contact forces [23, 24] or wind. In [25], the simultaneous online estimation of aerodynamic and contact forces is studied to discriminate between them and compute the wind velocity by means of model inversion. However, disturbance observers have not been used for ground effect estimation.

The influence of ground effect has been considered in the development of controllers for low-altitude flight in [26] using an adaptive controller and a height estimator that works well in the experiments, although false measurement from the ultrasonic sensor can destabilize the system. A take-off and landing controller that uses an ant colony filter for estimation of the ground effect is presented in [27]. The algorithm is tested in simulation with PID and sliding modes controllers, and in both cases the consideration of the ground effect improves significantly the controller performance. In [28], a PID landing controller with a ground effect robust compensator has been presented. The experimental tests show that accounting for the ground effect improves the controller behavior. Also, ground effect estimation using a vision sensor to estimate distance to obstacles and learning from previous flights have also been proposed [29]. A dynamic controller for rotorcraft landing and hovering in ground effect using feedback control based on flow field estimation has also been developed and tested in simulation [30].

However, in almost all cases, the model of the ground effect in [11] is assumed or evaluated for a single rotor. The only experimental results that have been reported, making experiments with a small quadrotor flying in hover over the ground at different heights [31] and using a test bench [32], suggest that the ground effect in multirotors may be larger than predicted by [11], although the issue has not been further analyzed.

This paper studies the influence of the ground effect in multirotor control, considering the full multirotor and not only an isolated rotor. Then, the effects of all the rotors of the multirotor being under the ground effect are analyzed. Furthermore, a phenomenon that we have called *multirotor partial ground effect* is described and analyzed. It appears only in multirotors when flying close to surfaces or objects in the environment, in situations where some of the rotors experiment the ground effect but not all. To the authors' knowledge, this is the first time that the aerodynamic partial ground effect is reported in the literature.

A test bench has been built to determine experimentally the influence of proximity to these surfaces of the individual rotors in a multirotor and of the whole multirotor. In the paper, the results of these experiments are presented.

The organization of the rest of the paper is as follows: Section 2 presents the analysis of the ground effect for a single rotor and the full multirotor and when only some of the rotors are under the ground effect, using experimental results in the test bench. Section 3 studies the implications of flying near surfaces for multirotor control, presenting simulations of different control strategies in ground effect. These control strategies include a standard linear controller, whose behavior is used as baseline for comparison, and two controllers that consider the ground effect: a controller that uses an external wrench disturbance observer for ground effect estimation and a controller that estimates ground effect from the model of the environment. Section 4 presents several experiments with multirotors in a test stand and flying

outdoors which show the ground effect and the performance of the controllers.

2. The Ground Effect in Rotary Wing UAVs

2.1. Ground Effect for Single Rotor. As mentioned before, the ground effect for single-rotor helicopters has been extensively studied in the literature [11–16]. When the rotor is under the ground effect, there is an increment in the thrust generated by the rotor for the same power, which is greater the closer the rotor is to the ground. In general, the ground effect in helicopters has been found to be significant when the rotor is at a vertical distance to the ground of up to one rotor diameter. A simple analytical model that is used to model the ground effect in helicopters uses potential flow with a single source to model the rotor airflow and the method of images to model the ground effect (potential flow with the method of images (PFI)) [11]. Other authors have presented empirical expressions for the increment of rotor thrust in ground effect which show similar results [16, 17], although the PFI model in [11] has been widely used because it has a simple analytical form and has been experimentally shown to accurately capture the relationship between rotor thrust in ground effect and rotor height over the ground surface.

The PFI model represents the rotor as a three-dimensional potential source, which has a strength of $s = R^2 v_{\mathrm{IGE}}/4$, where R is the radius of the rotor and v_{IGE} is the induced velocity at the rotor. The velocity potential of a source placed at (x_0, y_0, z_0) can be expressed as

$$\phi = -\frac{s}{\sqrt{(x-x_0)^2 + (y-y_0)^2 + (z-z_0)^2}}. \quad (1)$$

The effect of the ground plane is modelled as a mirror-image source to enforce that the flow does not pass through the ground plane. Thus, placing two sources in $x_0 = 0$, $y_0 = 0$, and $\pm z$ and obtaining the ratio of air velocities in-ground-effect (IGE) and out-of-ground-effect (OGE), the following expression for the rotor thrust increment due to the ground effect can be derived [11]:

$$\frac{T_{\mathrm{IGE}}}{T_{\mathrm{OGE}}} = \frac{1}{1-(R/4z)^2}, \quad (2)$$

where T_{OGE} is the thrust generated by the rotor flying out of the ground effect, T_{IGE} is the thrust when the rotor is under the ground effect, R is the radius of the rotor, and z is the vertical distance of the rotor to the ground.

In order to check the validity of this model for multirotor rotors, a series of tests have been performed in a specially designed test bench, which has been built for experimental motor/rotor characterization close to surfaces. This test bench, shown in Figure 2, is able to measure rotor thrust, rotor speed, and motor PWM input, controlled from a computer with a data acquisition card and a graphic user interface. The test bench allows making tests with different distance/inclination angle of the rotor plane with respect to surfaces.

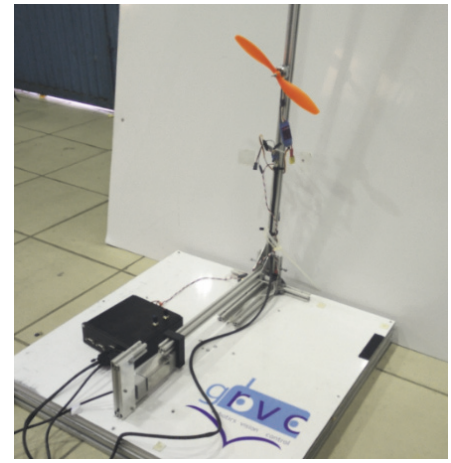

(a)

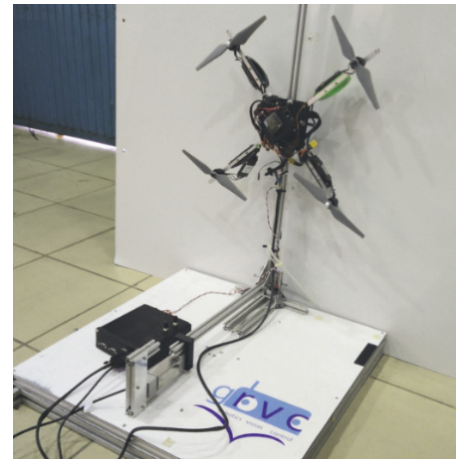

(b)

Figure 2: Test bench developed at GRVC for testing the ground effect. The "ground plane" (vertical white panel) can be placed at different distances from the rotor plane: (a) test with a single rotor and (b) test with a complete multirotor.

Tests with several combinations of motor and rotor have been made using the test bench. Figure 3 shows the results of two of them, which correspond to two multirotors of different size. The first one is the PQUAD quadrotor with four rotors of 12 cm radius and a total weight of 1,4 Kg, and the second one is the AMUSE multirotor [6], which has eight rotors of 20,5 cm radius and a total weight of 12 Kg. The ground plane has been placed at different distances from the rotor and a set of nine tests have been performed for each distance. The results are displayed in Figure 3 as the mean value of the increment in thrust with respect to the case when there is no ground effect ($T_{\mathrm{IGE}}/T_{\mathrm{OGE}}$) and an error bar showing the standard deviation.

The results in Figure 3 show that the PFI model that is used in helicopters for modelling the ground effect predicts also well the influence of the ground for multirotor rotors, which are much smaller.

A functional interpretation of the ground effect as seen in Figure 3 is that the ground "pushes the rotorcraft up" as the

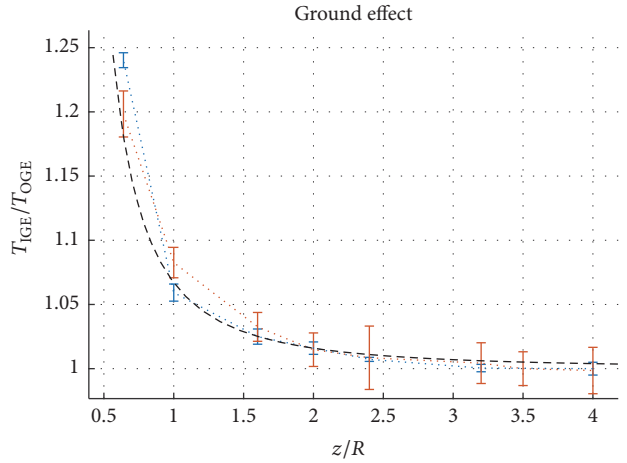

FIGURE 3: Ground effect for a single rotor: experimental and theoretical results of the increment in the thrust generated by a single rotor as a function of the distance to the ground plane. Black dashes lines represent the results of the PFI model. Blue error bar is the experimental result for PQUAD and orange error bar is the experimental result for AMUSE.

rotor approaches the surface. For the same transmitted power to the motor, the rotor develops more thrust caused only by the presence of the ground, which deviates the airflow radially and parallel to the ground, generating new fields of velocity and pressure around the rotor.

2.2. Ground Effect for the Full Multirotor. Unlike helicopters that have a single main rotor, in multirotors, the presence of multiple coplanar rotors may induce different behavior with respect to the single-rotor case, since the airflows from the different rotors may interfere with each other. An analytical model of the ground effect obtained using potential flow and the method of images for a full multirotor has been derived, following the same assumptions of the PFI for a single rotor shown in the previous subsection. The potential flow model uses one source located at the geometric center of each rotor and its corresponding image source to represent the ground boundary conditions. So, the four rotors and four images will be modelled, placing three dimensional sources in the same way as the previous section. For the case of a quadrotor with four coplanar rotors with a separation d from each rotor axis to its adjacent rotor axes, the sources of the rotors and its images will be $\phi_{1,5} : (0, 0, \pm z)$, $\phi_{2,6} : (0, d, \pm z)$, $\phi_{3,7} : (d, 0, \pm z)$, and $\phi_{4,8} : (d, d, \pm z)$, where $\phi_{i,i+4}$ represents the velocity potentials of the rotor i and its rotor image $(i + 4)$. Thus, the resultant expression of the increment in thrust due to the ground effect is the following:

$$\frac{T_{IGE}}{T_{OGE}} = \frac{1}{1 - (R/4z)^2 - R^2\left(z/\sqrt{(d^2 + 4z^2)^3}\right) - (R^2/2)\left(z/\sqrt{(2d^2 + 4z^2)^3}\right)}. \quad (3)$$

Figure 4 shows the increment in thrust for a quadrotor due to the ground effect with a dashed line and for a single rotor with a solid line for comparison. It can be seen that the effect is significantly larger for a quadrotor due to the aerodynamic interference of the other rotors (the additional terms in the denominator of (3)).

Furthermore, experimental tests with a full quadrotor have also been performed using the test bench described above. In this case, the tests have been done with the PQUAD quadrotor shown in Figure 2(b), and the results can be seen in Figure 4. Similar to the single-rotor case, five tests have been done at each distance to the ground, and the average values are marked with a red circle and a blue error bar represents the standard deviation. The experimental results in Figure 4 give values for the ground effect thrust increase which are significantly larger than the predicted ones with the PFI quadrotor model (dashed line) and the results for a single rotor. A possible explanation for this larger effect in the full multirotor is what is known as the *fountain effect*, which arises when a pair of rotors are flying close to the ground. This can lead to strong flow interactions of the slipstream flow between the rotors. The airflow of each rotor splays out radially in all directions when it encounters the ground plane, but in the area between the rotors it interacts with the flow of the other rotor and the flow reverses back up through the rotors, impinging on the central part of the quadrotor body, increasing the upward force acting on the aerial vehicle due to the ground effect. This effect has been reported for tandem helicopters [33] and has been suggested also for quadrotors [32]. Figure 5 shows a CFD simulation that illustrates this fountain effect. This simulation has been done using a simplified model of a quadrotor hovering at a distance of $2R$ (with a rotor radius R of 12 cm for the simulation) from the ground plane. The rotors have been modelled as a constant velocity source on the rotor area, that is, the rotation of the propeller is not being simulated. The velocity of the constant velocity source is the mean value of the airspeed measured experimentally under the rotors of the PQUAD quadrotor flying in hover. The central part of the quadrotor body has been modelled with a solid box. Figure 5 shows the velocity field in a vertical plane cut along the quadrotor diagonal. It can be seen in this figure that the airflow coming out from the rotors, instead of spreading parallel to the ground in all directions as in the outer part of rotors 1 and 3, interacts with the ground and the central body in the central area between both rotors, forming a vortex ring that causes the fountain effect with the increase of the thrust due to the ground effect.

The PFI quadrotor model of (3) does not reproduce the behavior observed in the experiments. Since it is very useful to have a simplified model of the ground effect in multirotors

that can be used for simulations and controller development, an additional term has been included in the equation to account for flow recirculation and the central body lift that it generates. This additional term uses the velocity of the air at the central point of the body and adjusts its influence with an empirical coefficient K_b, which takes a value close to 2 in the experiments performed. Then the expression of the thrust increment due to the ground effect takes the following form:

$$\frac{T_{\mathrm{IGE}}}{T_{\mathrm{OGE}}} = \frac{1}{1-(R/4z)^2 - R^2\left(z/\sqrt{\left(d^2+4z^2\right)^3}\right) - \left(R^2/2\right)\left(z/\sqrt{\left(2d^2+4z^2\right)^3}\right) - 2R^2\left(z/\sqrt{\left(b^2+4z^2\right)^3}\right)K_b}, \quad (4)$$

where b is the distance between two opposite rotor axes (diagonal) and K_b is the empirical body lift coefficient. Figure 6 shows the thrust increment due to the ground effect given by the multirotor PFI with the body lift term, with $K_b = 2$. As can be seen in the figure, expression (4) matches more closely the experimental values.

As a conclusion, although the ground effect in multirotors (multiple coplanar rotors) has been assumed by most researchers to be the same as for helicopters (a single rotor) [18–29] and be significant up to distances to the ground of 2 rotor radii, the results presented in this section show clearly that this is not the case; the ground effect for multirotors is much larger, being significant for distances to the ground of up to 5 rotor radii. Although the PFI can be expanded to include the contributions of all the rotors of a quadrotor (see (3)), the addition of a body lift term with an empirical coefficient (see (4)) reproduces the experimental behavior and can be used in simulations and controller development.

2.3. Partial Ground Effect. A new phenomenon that appears in aerial manipulation with multirotors when approaching some locations in the environment to manipulate objects is what we called *multirotor partial ground effect*. In the partial ground effect (see Figure 7 for a quadrotor), which is unique to multirotors, the multirotor is flying in hover or at low speed in a situation in which only one or several of its rotors (but not all) are under the influence of the ground effect. In this situation, rotor 3 in Figure 7 will experiment an increase in thrust ΔT_{ge1} which will generate a disturbing moment M_{ge1} which tries to rotate the multirotor counterclockwise and then move apart from the object because of the tilting. This effect may induce an important disturbance, and its implications in multirotor control will be analyzed in the next sections.

If one of the rotors is under the ground effect, its characterization can be modelled as described in Section 2.1. However, the case when three of the rotors are close to a horizontal surface under the ground effect will be different. For this case, a similar analysis to the full multirotor has been made, including the PFI analytical model and the experimental tests in the test bench with a quadrotor with only three rotors switched on. The results are shown in Figure 8, where the ground effect is much larger than that for a single rotor and follows the same trend as that for the full multirotor, though with less intensity.

2.4. Response to Attitude Disturbances. Another consequence of the ground effect which is also unique to multirotors comes from the way the rotor thrust forces vary with the distance to the ground. In Figure 9, a multirotor hovering in ground effect which experiments an attitude perturbation is shown. Since the increment in rotor thrust depends on the distance of each rotor to the ground and each rotor has a different distance (z_1 and z_3 in Figure 9), a disturbance moment M_{ge2} will be generated which tries to rotate the multirotor opposing the disturbance, and, thus, it is a stabilizing moment.

In practice, however, it has been found that for typical attitude disturbances of about 5–10° this effect, although stabilizing, is not considerable unless the multirotor is very close to the ground, and then it is considered not significant for controller development.

3. Influence of Proximity to Surfaces in Multirotor Control

This section analyzes the influence of flying close to surfaces on multirotor control. Partial ground effect is a special phenomenon that appears only in multirotors when flying close to surfaces and can be defined as situations in which only some of the rotors (but not all) are under the ground effect. We study the control of the partial ground effect because it is the most related to the practice of aerial manipulation. The section includes a comparative study of the results obtained in simulation tests of different control strategies of a quadrotor model. The tests have been made simulating that the multirotor is under the influence of the ground effect and using the ground effect model presented in the previous section.

3.1. Multirotor Dynamic Model. The dynamic model of the multirotor can be obtained using the Euler-Lagrange formulation [34, 35]. This model is basically obtained by considering the multirotor as a rigid body evolving in 3D space and subject to one force (the total thrust generated by al the rotors) and three moments generated by the differences in speed and thrust of pairs of rotors. The dynamics of the electric motors are relatively fast and therefore they will be neglected as well as the flexibility of the blades.

The generalized coordinates of the multirotor can be defined as

$$q = (x, y, z, \phi, \theta, \psi), \quad (5)$$

where $\xi = (x, y, z)$ denote the position of the center of mass of the multirotor relative to the inertial frame and

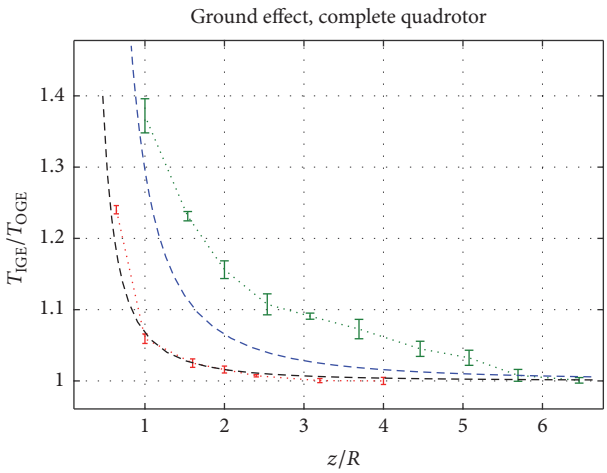

FIGURE 4: Ground effect for a full multirotor (quadrotor): experimental and theoretical results of the increment in the thrust generated by a quadrotor as a function of the distance to the ground plane in green error bar compared to the results for a single rotor in red error bar. The PFI approximations are represented in blue and black dashed lines, respectively.

$\eta = (\phi, \theta, \psi)$ are the three Euler angles (roll, pitch, and yaw) representing the orientation of a reference system attached to the multirotor body with respect to the inertial frame. If m is the total mass of the multirotor and J is the matrix of moments of inertia of the aerial vehicle in the inertial frame, the resultant Euler-Lagrange equations for the translational and rotational degrees of freedom are, respectively,

$$m\ddot{\xi} + \begin{pmatrix} 0 \\ 0 \\ mg \end{pmatrix} = RF_{\xi}, \qquad J\ddot{\eta} + C_1(\eta, \dot{\eta})\dot{\eta} = \tau. \tag{6}$$

In (4), $C_1(\eta, \dot{\eta})$ is referred to as the Coriolis terms and contains the gyroscopic and centrifugal effects, R is the rotation matrix between the body and inertial systems, and $F_{\xi} = (0, 0, T)$ and $\tau = (\tau_{\phi}, \tau_{\theta}, \tau_{\psi})$ are the force and moments generated by the rotors. Both translational and rotational dynamic equations can be expressed in matrix form as

$$M(q)\ddot{q} + C(q, \dot{q})\dot{q} + G(q) = F, \tag{7}$$

where $F = (F_{\xi}, \tau)$ are the generalized moments and M, C, and G are the mass, Coriolis, and gravity matrix, respectively. The thrust generated by each rotor and the reaction torque due to rotor drag are generally accepted to be proportional to the square of the angular velocity of the rotor ω_i when flying on free air:

$$T_i = k\omega_i^2, \qquad Q_i = c\omega_i^2. \tag{8}$$

The thrust and drag coefficients k and c can be determined by static thrust tests. Then, for a quadrotor in which the distance of the geometric center to the axis of each rotor is d, there is a direct correspondence between the four generalized moments and the angular velocities of the rotors:

$$\begin{bmatrix} T \\ \tau_{\phi} \\ \tau_{\theta} \\ \tau_{\psi} \end{bmatrix} = \begin{bmatrix} k & k & k & k \\ 0 & kd & 0 & -kd \\ -kd & 0 & kd & 0 \\ -c & c & -c & c \end{bmatrix} \begin{bmatrix} \omega_1^2 \\ \omega_2^2 \\ \omega_3^2 \\ \omega_4^2 \end{bmatrix}. \tag{9}$$

However, when the multirotor is flying close to the ground or other horizontal surfaces, the rotor thrust and drag model (8) are no longer valid, as has been shown in Section 2. To account for the ground effect and partial ground effects in the simulator, the thrust model is modified as

$$T_i = k\omega_i^2 f_{GE}(z_{r,i}), \tag{10}$$

where $f_{GE}(z_r)$ is the ground effect factor that accounts for the increment in thrust due to the ground effect and partial ground effect, which is obtained from the data in Sections 2.1–2.3. This ground effect factor, $f_{GE}(z_r)$, depends on the relative distance of each rotor to the ground, z_r. For that purpose, a 3D map of the environment in which the aerial robot is flying has been included in the simulator (see Figure 10). Furthermore, in the simulator, we have considered the fact that the rotor thrust increment varies approximately linearly with the rotor area that is under the ground effect, as has been reported with experiments with a helicopter rotor [36].

Then, the generalized dynamic model of the multirotor becomes

$$M(q)\ddot{q} + C(q, \dot{q})\dot{q} + G(q) = F + F_{GE}, \tag{11}$$

where F_{GE} are the additional generalized moments due to the ground effect.

Two different cases have been tested in order to analyze the influence of the ground effect in multirotor control and compare the different control approaches.

(1) The multirotor flies over an obstacle (see Figure 11(a)), beginning in point A and ending in point B. In the reference trajectory, the y-coordinate remains constant, and the x-coordinate varies from $x = 0$ (point A) to $x = 7$ (point B). The obstacle is between $x = 3$ and $x = 5$.

(2) The multirotor is commanded to go from point A to point B and hover on B, where it has to perform a manipulation operation (see Figure 11(b)). In point B, only one rotor is over the obstacle and then under the influence of the partial ground effect. In the reference trajectory, the y-coordinate remains constant, and the x-coordinate varies from $x = 0$ (point A) to $x = 2.8$ (point B). The obstacle is between $x = 3$ and $x = 5$.

Three different control alternatives have been analyzed in both scenarios: conventional control with cascaded linear controllers, estimated torque controller, and control with rotor height estimation (feedforward). The results obtained using the different control alternatives are shown below. A comparison between these alternatives will be shown at the end of this section.

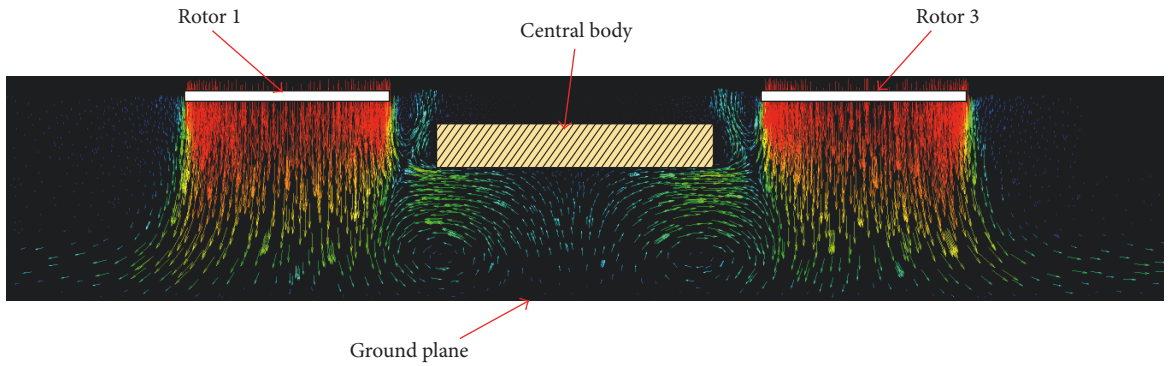

Figure 5: CFD simulation of a quadrotor simplified model hovering in ground effect at a distance of $2R$ of the ground plane. The rotors have been modelled as a constant velocity source on the rotor area, with the mean velocity measured experimentally on the PQUAD quadrotor flying in hover.

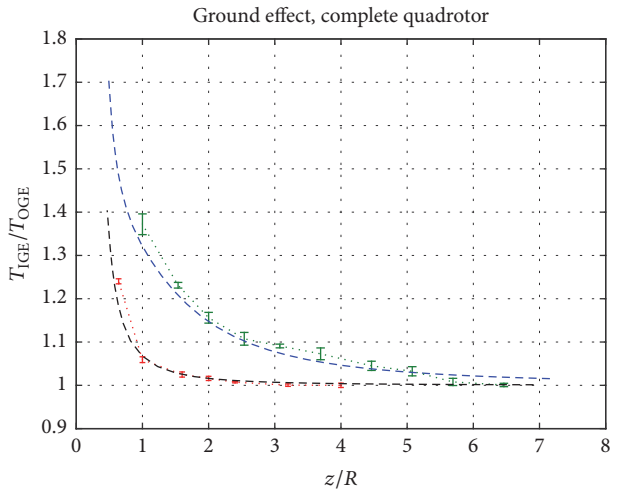

Figure 6: Ground effect for a full multirotor (quadrotor): experimental and theoretical results of the increment in the thrust generated by a quadrotor as a function of the distance to the ground plane (green) compared to the results for a single rotor (red). Five experiments have been performed at each distance; the error bar represents the standard deviation. PFI approximations are represented in the blue dashed line for quadrotor with body lift term (see (4)) and black dashed line for one rotor (see (2)).

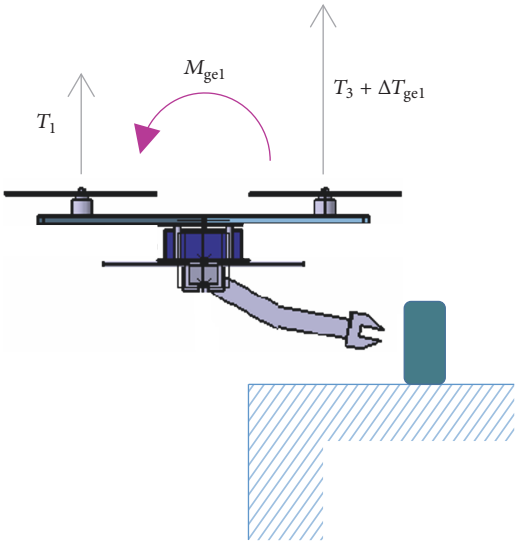

Figure 7: Multirotor under partial ground effect.

3.2. Conventional Control. A standard control scheme with cascaded PID linear controllers in each channel has been considered to analyze the response of the system to a conventional controller which does not take the ground effect into account. This control scheme is widely used as baseline in multirotor autopilots [37], and it is a good reference for the comparison with other methods. The multirotor is moving forward along the x global axis and the yaw angle is maintained constant in the simulations, and so the relevant variables that are presented in the plots as a function of the time are the pitch angle, θ, and the global coordinate in the direction of motion, x.

The results obtained in the simulation using the PID controller in the two experiments are shown in Figure 12 (case 1: flying over obstacle) and Figure 13 (case 2: hovering in partial ground effect). In the figures, a broken line has been included to mark the x-coordinate of the final destination of the multirotor (point B in both cases). Furthermore, the values of the x-coordinates that are over the obstacle are highlighted with green background. Several simulations are presented in each plot for comparison: "OGE," which is the simulation of the multirotor flying high above the obstacle, so that no ground effect is present, and two simulations flying close to the obstacle ("IGE") at two different heights normalized with the rotor radius R.

Figure 12 shows the evolution of the x-coordinate and the pitch angle for the first case: flying over an obstacle. It can be observed that the ground effect disturbance produces a torque that affects the system in attitude and position. This torque is more significant when the vehicle is closer to the obstacle. In fact, the results for $z/R = 2.0$ show how this torque pushed the vehicle away from the obstacle repeatedly and it cannot fly over it with this controller.

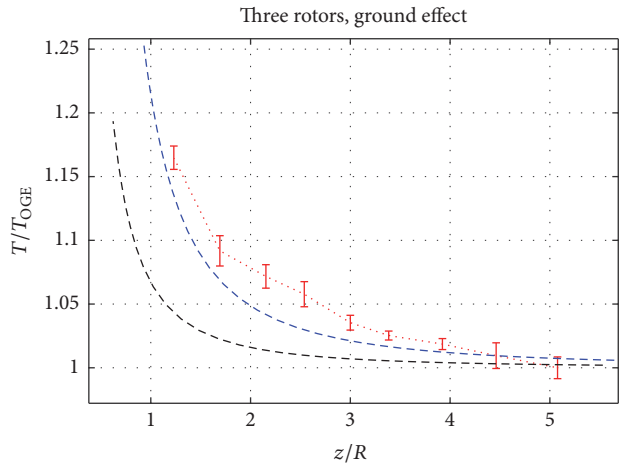

Figure 8: Red error bar: experimental and theoretical results of the increment in the thrust generated by three rotors as a function of the distance to the ground plane. Black dashed line: theoretical results of the PFI method for a single rotor. Blue dashed line: theoretical results of the PFI method for three rotors.

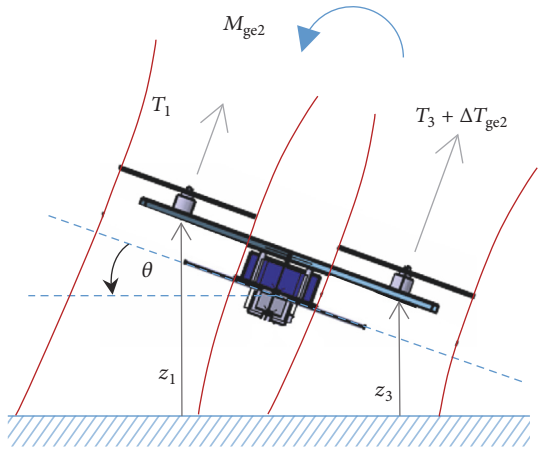

Figure 9: Response of a multirotor in ground effect to attitude disturbance.

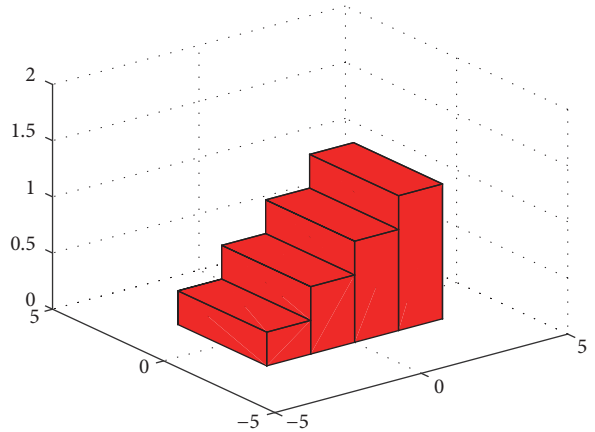

Figure 10: Example of environment map for simulation.

In the second case (Figure 13), the multirotor tries to hover with only one rotor over the obstacle, but it is unable to do it in the x reference and keeps flying in a maintained oscillation going in and out of the ground effect.

The simulations presented in Figures 12 and 13 were performed with the quadrotor flying at a velocity of 0.2 m/s. In order to assess the behavior at different translational velocities, the simulations have been done at a maximum speed of 1 m/s. Figure 14(a) shows the results of the hovering in partial ground effect test case, and it can be seen that the behavior is similar to the one presented in Figure 13. Figure 14(b) shows the simulation of case 2: flying over obstacle. In this case, although there is a strong perturbation in the pitch angle, the inertia of the multirotor moving at 1 m/s allows it to surpass the obstacle unlike when flying at 0.2 m/s. Since moving at a slow speed is more restrictive and also is more appropriate for aerial manipulation tasks, the rest of the simulations will be done with the multirotor flying at 0.2 m/s.

Other simulations have been done considering sensor noise. Figure 15 shows the simulation of the quadrotor in case 1: hovering in partial ground effect with a velocity of 1 m/s and $z/R = 2$. A normal distribution with a standard deviation of 0.015 rad/s has been supposed for the noise in the gyroscopes. It can be seen in Figure 15 that the presence of noise in the sensors amplifies the oscillations, although the qualitative behavior is similar. In the rest of the paper, only the noise-free simulations will be presented.

3.3. Estimated Torque Controller. This control alternative includes a torque disturbance observer that is used to estimate the torque induced by the partial ground effect, caused by the different aerodynamic thrust generated by the rotors when the multirotor is in partial ground effect. Several approaches have been used to estimate external force and torque disturbances in multirotors [22–24, 38]. In this paper, a nonlinear torque disturbance observer has been implemented [24]. If the multirotor dynamic equations are expressed in compact form (11), the nonlinear observer is able to estimate the forces and torques due to the ground effect F_{GE}:

$$\begin{aligned}\dot{\widehat{F}}_{GE} &= L(q,\dot{q})\left(F_{GE} - \widehat{F}_{GE}\right) \\ &= -L(q,\dot{q})\,\widehat{F}_{GE} \\ &\quad + L(q,\dot{q})\left(M(q)\,\ddot{q} + C(q,\dot{q})\,\dot{q} + G(q) - F\right),\end{aligned} \tag{12}$$

where $\widehat{F}_{GE}$ is the vector of estimated force and torque disturbances due to the ground effect and $L(q,\dot{q})$ is the observer matrix that has to be designed in order to assure convergence of the observer. Figure 16 shows the control scheme of this strategy.

The results obtained with this control approach are shown in Figure 17 (flying over an obstacle) and Figure 18 (hovering in partial ground effect). In these figures, it can be observed that the obtained results are better than using a conventional PID-based controller, as was expected.

In the first test case (as defined in Figure 11(a)), the response of the system is faster than with the baseline controller. Moreover, the multirotor is able to avoid being

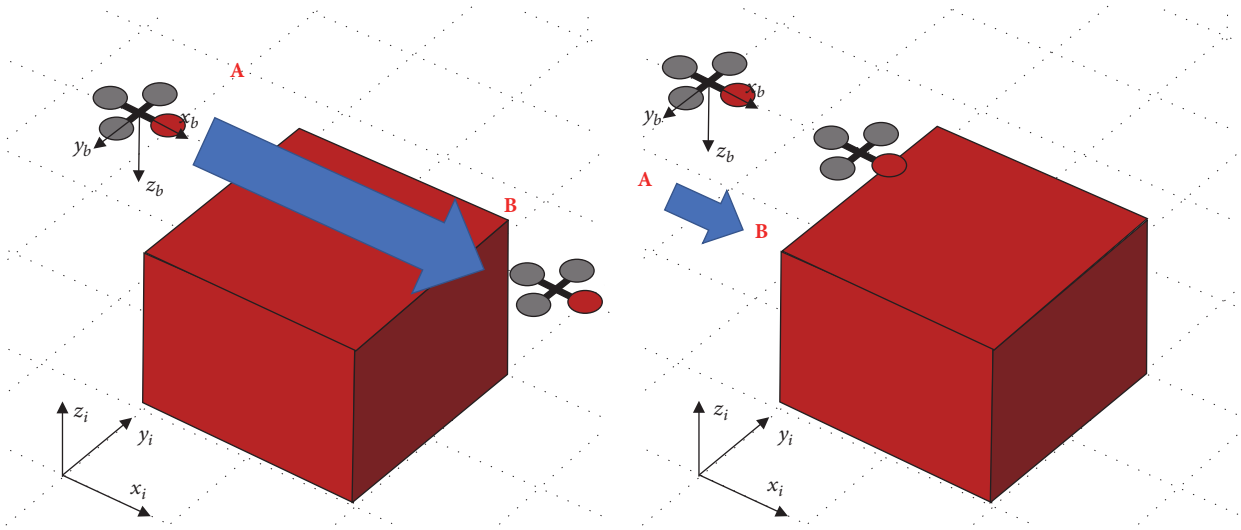

Figure 11: (a) Case 1: flying over an obstacle under the influence of the ground effect. (b) Case 2: hovering at a point with only one rotor under the influence of ground effect.

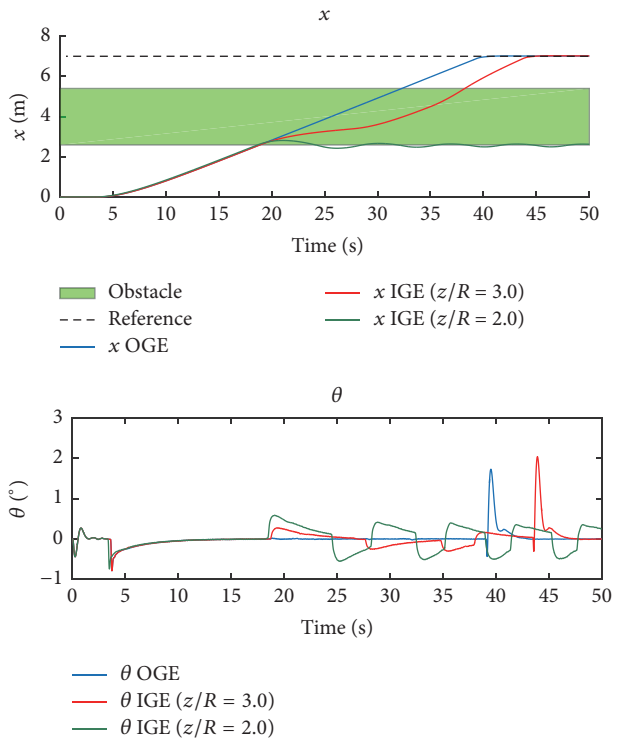

Figure 12: PID controller: flying over obstacle.

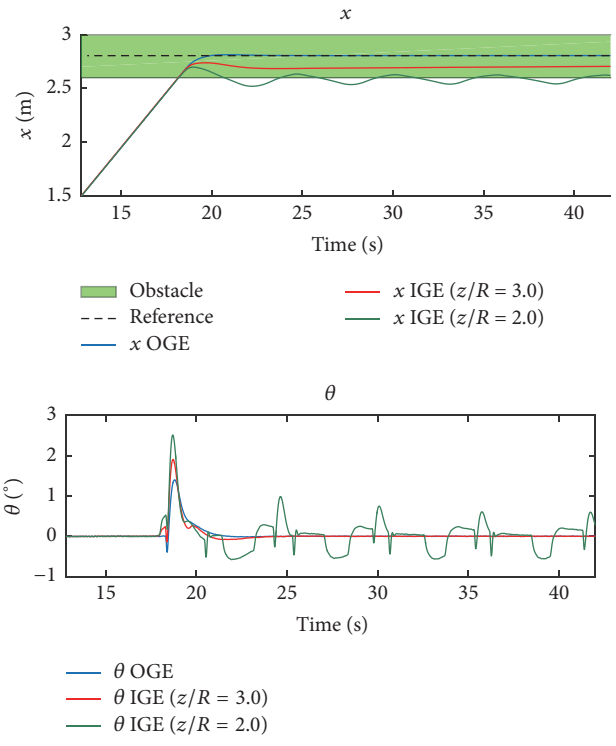

Figure 13: PID controller: hovering in partial ground effect.

pushed away from the obstacle when $z/R = 3.0$, and it is able to arrive to its destination at point B ($x = 7$) when it is flying closer to the obstacle at $z/R = 2.0$.

The results of simulations in the second case (Figure 18) show that this control alternative can eliminate the aggressive oscillations in pitch angle.

The estimated torque controller can improve the response of the system because the disturbances are partially cancelled at the same time they are being produced.

3.4. Control with Rotor Height Estimation (Feedforward). The last alternative that has been studied is based on a feedforward concept. As has been seen in the previous sections, the ground

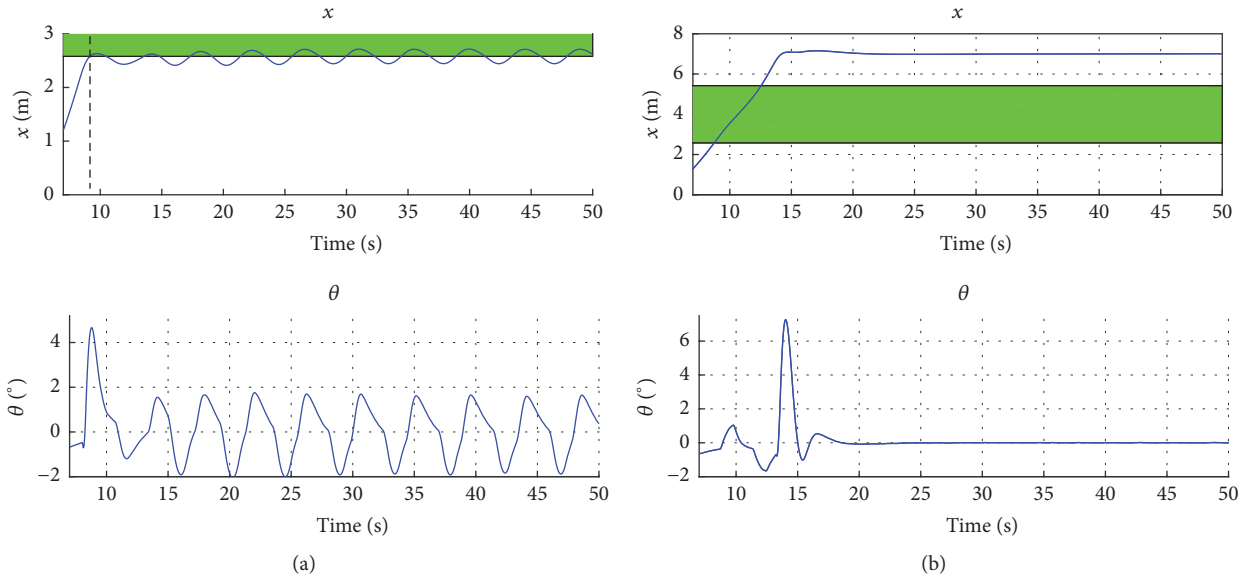

Figure 14: PID controller: velocity of 1 m/s and $z/R = 2$. (a) Hovering in partial ground effect. (b) Flying over obstacle.

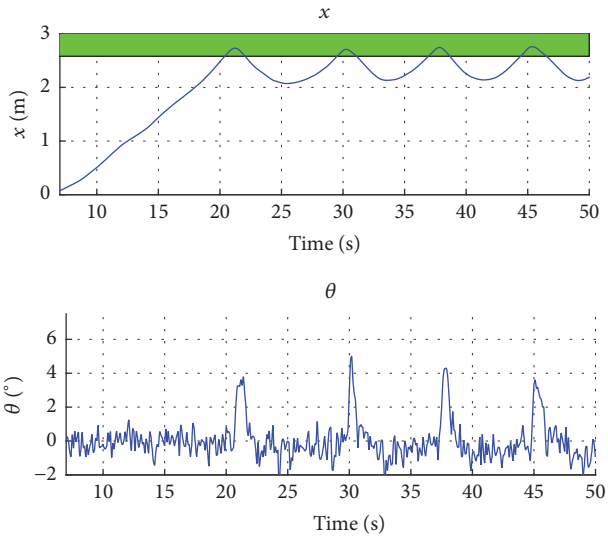

Figure 15: PID controller: hovering in partial ground effect. Simulation with sensor noise.

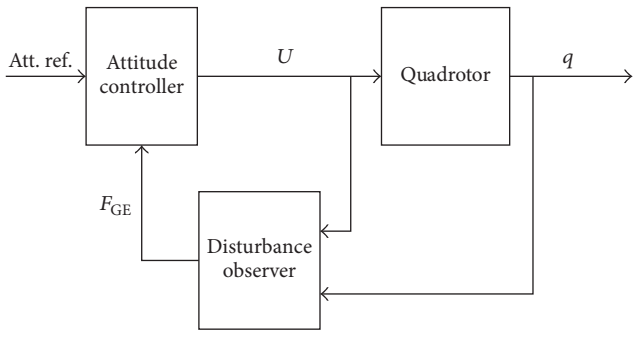

Figure 16: Estimated torque controller.

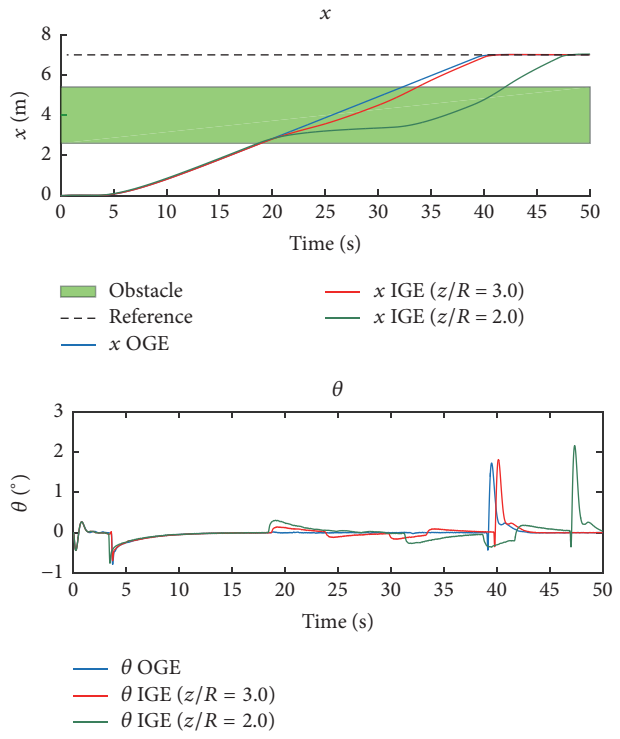

Figure 17: Estimated torque controller: flying over an obstacle.

effect torque disturbance is directly related to the relative distance from the rotor to the ground or obstacle. Then, if we can have an estimation of this relative distance, it is possible to implement a feedforward control approach that allows canceling the torque disturbance partially. The block diagram of this approach is represented in Figure 19.

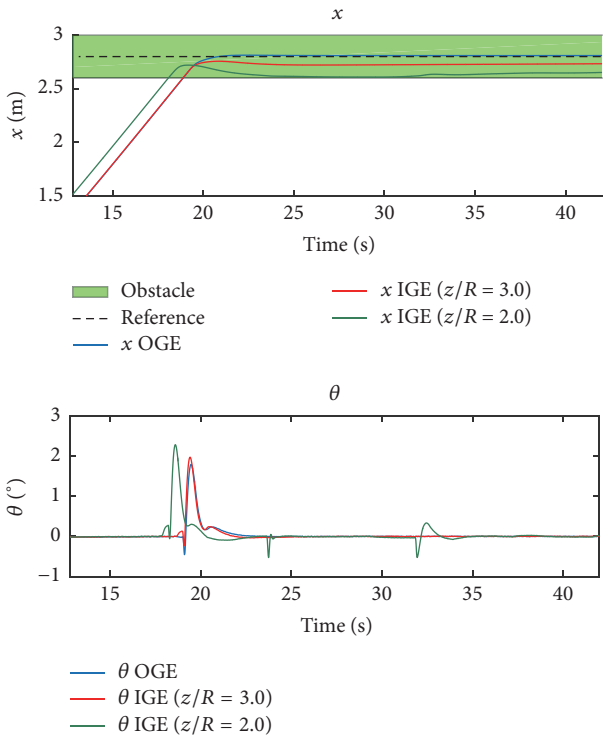

Figure 18: Estimated torque controller: hovering in partial ground effect.

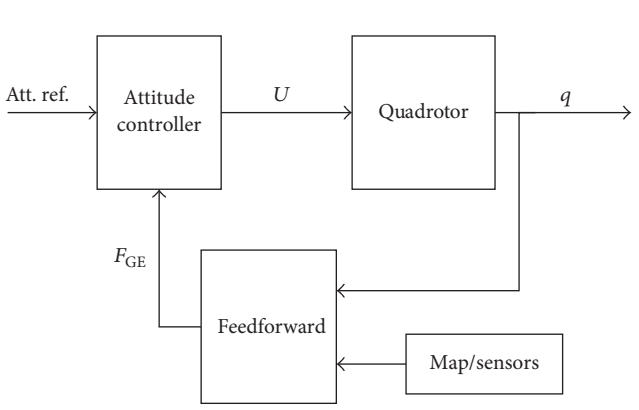

Figure 19: Control scheme of feedforward controller.

The results obtained in the simulation with the feedforward controller in the two experiments are shown in Figures 20 and 21. As can be seen in the Figures, the results are better than those obtained with the other control alternatives. This is because the torque disturbances can be anticipated, and the multirotor controller can compensate them largely.

It is important to mention that this strategy depends heavily on the availability of an accurate environment map and precise relative positioning with respect to the map. These errors can come from the estimation of the multirotor's relative height with respect to the terrain (z-error), although available sensors (i.e., laser altimeter or ultrasound range sensor) allow for a relatively accurate height estimation and their effect will be a deviation of the predicted thrust increase

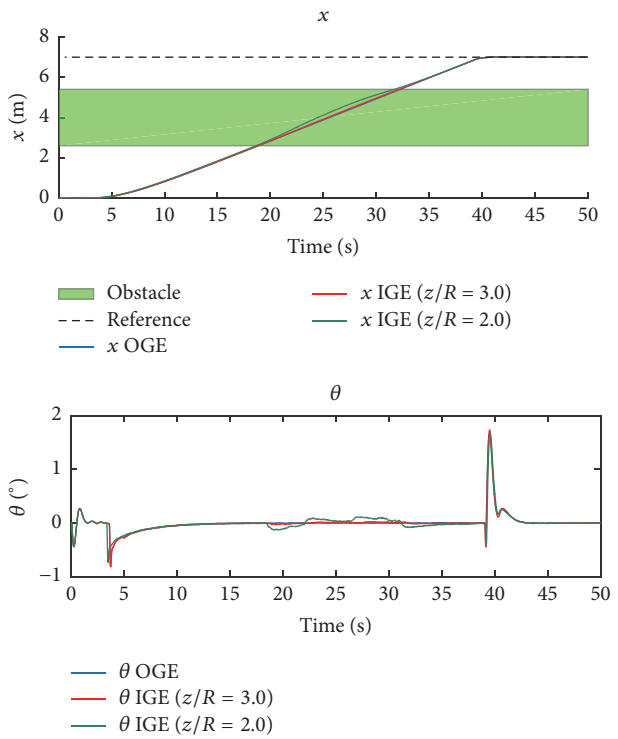

Figure 20: Feedforward controller: flying over obstacle.

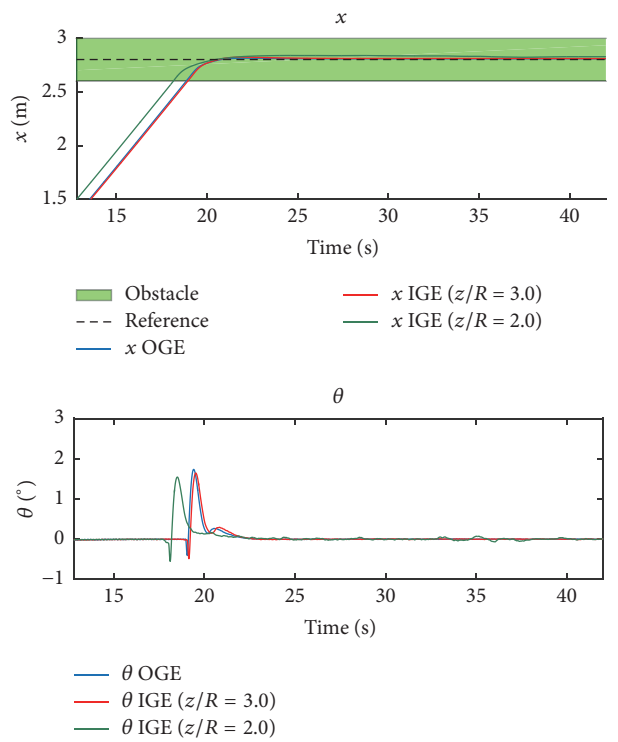

Figure 21: Feedforward controller: hovering in partial ground effect.

from the real one. Offset errors in the horizontal plane are more common, since precise UAV positioning outdoors is still a difficult task (small UAVs usually do not have cm-level

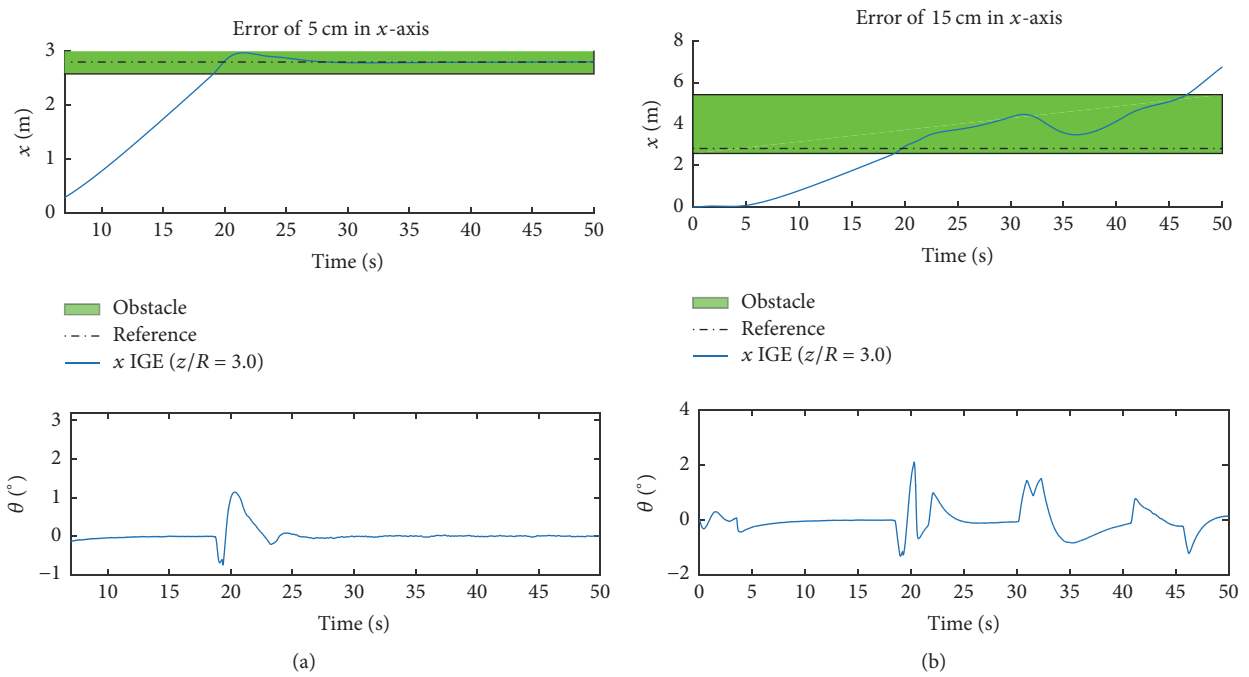

Figure 22: Simulation of feedforward controller using maps with offset errors: (a) 5 cm error and (b) 15 cm error.

DGPS RTK receivers), and the effect of these errors is the prediction of a thrust increase when it does not exist.

Different cases have been tested in simulation. Figure 22 shows the results when the map has an x-offset error, which can be compared to the results of Figure 21 (map without offset error). This offset error produces that the multirotor controller anticipates a thrust increase which does not exist yet, generating oscillations and instability. If the map has small errors, the controller will present an overshoot but still will be able to guide the UAV, as is shown in the simulation in Figure 22(a) (with an x-offset error of 5 cm added to the map). If the errors are larger, the oscillations can grow to instability, as shown in Figure 22(b), where the offset error added to the map is of 15 cm. In this case, the performance is even worse than using the standard PID control scheme (see Figure 13).

In practice, a sensor-based approach could be convenient to implement this type of controller, estimating in real time the relative distance of the rotors to the surfaces of the environment. One possibility is to use a sensor below each rotor which is able to measure the relative height, as ultrasonic sensors. Another option is to use exteroceptive sensors (laser and cameras) to build a map of the environment in real time and use this map to anticipate torque disturbances.

3.5. Comparison between Different Control Alternatives. Figure 23 (flying over obstacle) and Figure 24 (hovering in partial ground effect) present a comparison of the simulations with the different multirotor controllers, flying at a relative distance of $z/R = 2.0$ from the obstacle.

From the results in Figures 23 and 24, it can be seen that the conventional PID-based controller that is implemented in many multirotors does not give acceptable results when flying close to obstacles or the ground, causing oscillations that may lead to dangerous situations or even preventing the multirotor from reaching its destination because it gets trapped in a cycle at the beginning of the obstacle.

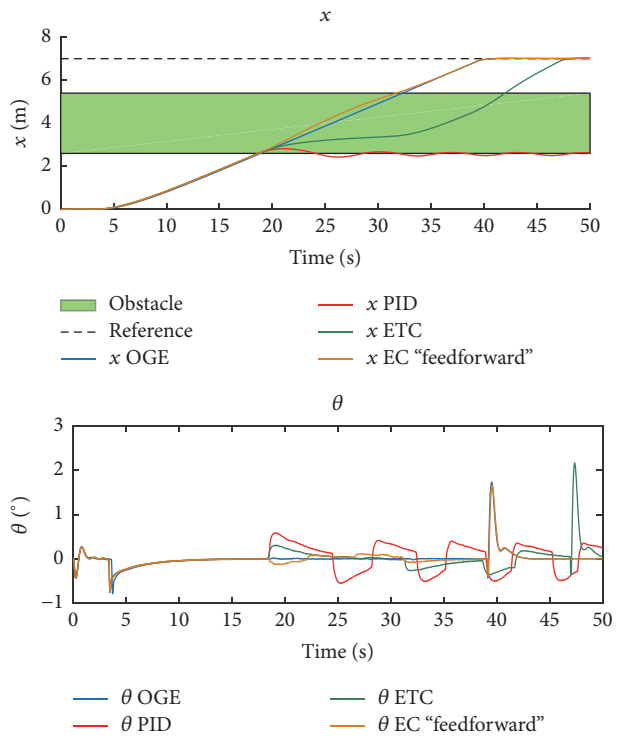

Figure 23: Flying over obstacle: comparison of controllers.

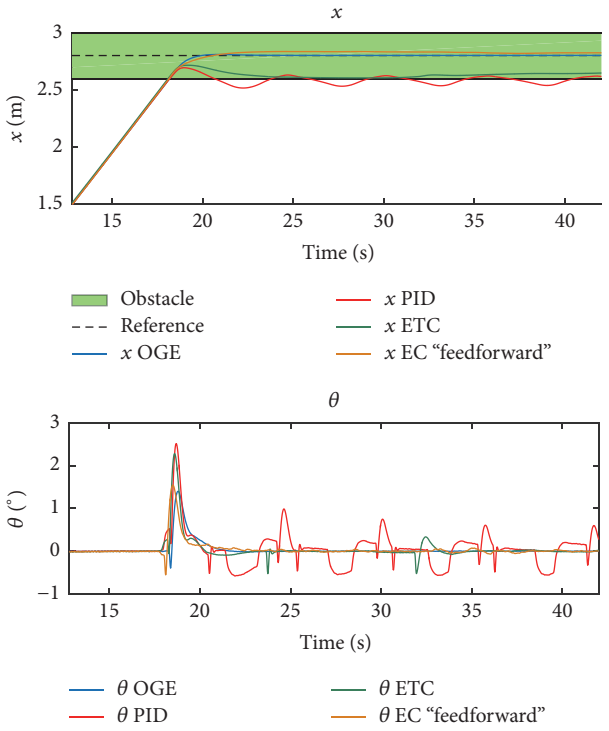

Figure 24: Hovering in partial ground effect: comparison of controllers.

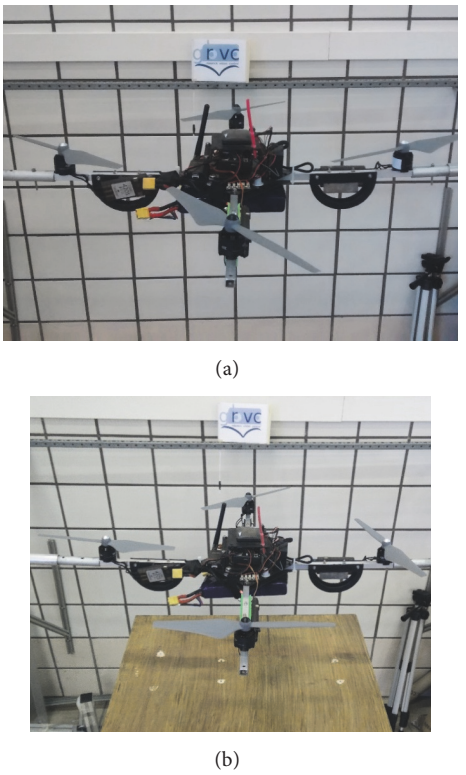

(a)

(b)

Figure 25: Experimental tests with multirotors in the test bench: (a) the PQUAD and (b) the PQUAD with a ground plane.

With a detailed environment map, the feedforward controller will give better results, provided that the practical implementation issues are correctly addressed.

4. Experiments

Several experiments have been made to assess experimentally the performance when the multirotor flies over an obstacle. A first set of experiments were done in a test bench in which the multirotor is allowed to rotate freely around one of the axes (pitch angle) (Figure 25(a)). The ground effect is introduced placing a large plate under one of the rotors at different distances (Figure 25(b)), while the multirotor pitch angle is controlled by the cascaded PID controller.

Figure 26 shows the results of the experiment placing the ground plate at $z/R = 2$ with both the PQUAD multirotor and the AMUSE aerial manipulator. The evolution of the pitch angle for both cases is presented in Figure 26 marking with green background the case when the ground plate is placed below one of the rotors. It can be seen that when the (partial) ground effect is present, the torque disturbance induces an increase in the pitch angle which is difficult to correct by the PID controller. Both experiments produced similar results; this is according to the experimental results obtained in Figure 3.

The next experiments were intended to demonstrate the viability of the control approaches presented in previous sections. A first test was performed implementing the feedforward control scheme, in which the feedforward term was activated by a switch in the radio of the safety pilot. It can be seen in Figure 27 that when the feedforward controller was not activated (Figure 27(a)), the induced pitch perturbation is similar to the results in Figure 26. However, in Figure 27(b), the feedforward controller was tested using the switch in the radio and the controller could maintain the pitch angle stably with much smaller variations.

A second test was performed, implementing the disturbance observer presented in Section 3.2. Figure 28 shows the time evolution of the pitch angle during the experiment. As in previous experiments, the green background corresponds to the ground plate placed under one rotor. As can be seen in Figure 28, after placing the ground plate, the pitch angle begins to increase, behaving similarly to the first experiments in Figure 26, but right after that, the disturbance observer is able to estimate the external wrench and the controller can effectively compensate it.

The last step in the experimental tests was to reproduce how the ground effect affects during a normal flight. Figure 29 shows two images of the experiment: the first one in free flight and the second one when a ground plane is placed under one of the rotors.

Figure 30 shows the evolution of the multirotor pitch angle and the reference during the experiment, in which the multirotor is being controlled with the standard PID cascaded controller, marking with green background the case when one of the rotors is under the ground effect (partial ground effect). It can be seen that initially the response is similar to the test bench experiments: the pitch angle suffers a perturbation

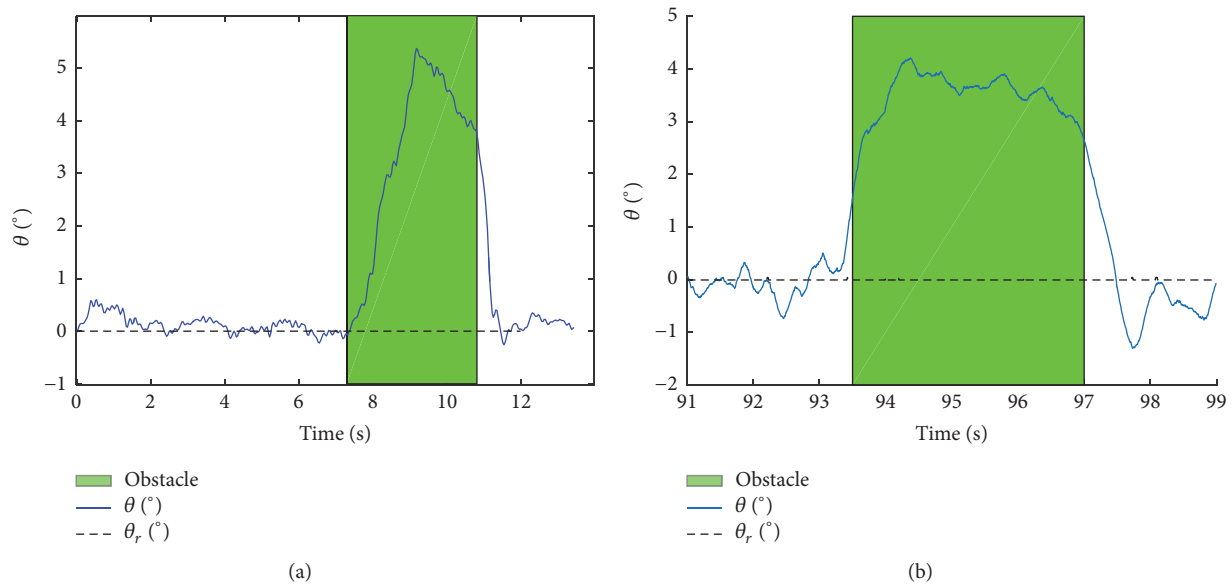

Figure 26: Experiments in the test bench: influence on the pitch angle of placing a ground plane under one of the rotors (green background). (a) Effect in the PQUAD multirotor. (b) Effect in the AMUSE multirotor.

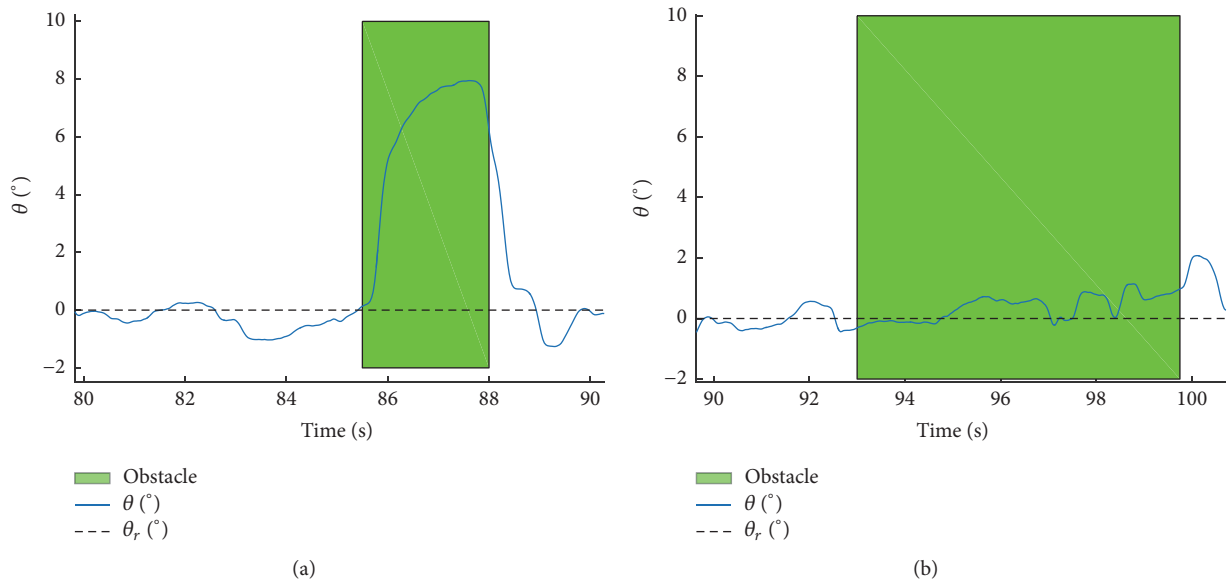

Figure 27: Experiments in the test bench: variations of the quadrotor pitch angle when placing a ground plane under one of the rotors (green background): (a) with the standard PID controller (not compensating) and (b) when the compensation is implemented (feedforward controller).

caused by the torque generated by the partial ground effect (different thrust forces of the same rotors for the same input signal). In this case, a perturbation appears in the opposite direction when the partial ground effect disappears, which was present in some of the test bench experiments but with smaller amplitude (see Figure 26(b) and Figure 27(a)). This can be due to several factors of flying outdoors, for example, wind gusts or turbulences. It also can be explained because the quadrotor is attached to the test bench at two points in opposite arms of the quadrotor, allowing it to rotate around the axis (see Figure 25), and the friction may dampen the oscillation.

5. Conclusions

This paper has shown the significance of the aerodynamic ground effects on multirotor systems. The quantification of this effect is very relevant in applications involving flight very close to surfaces as required in aerial manipulation. This paper has provided a precise characterization of the ground

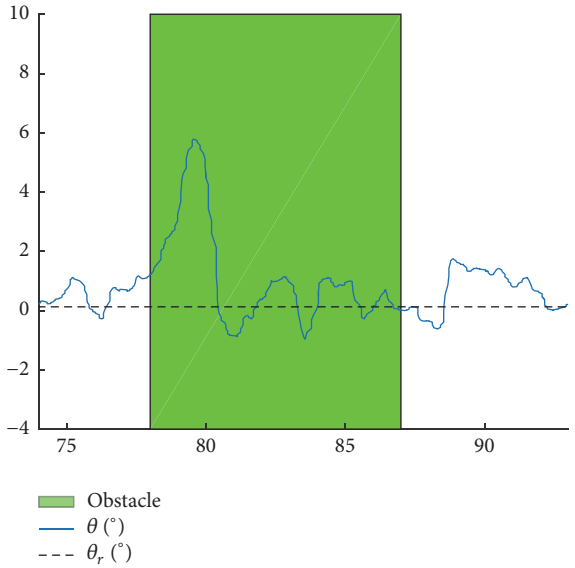

Figure 28: Experiments in the test bench: variations of the quadrotor pitch angle when placing a ground plane under one of the rotors (green background).

(a)

(b)

Figure 29: Partial ground effect tests with multirotor flying outdoors: (a) multirotor in free flight; (b) multirotor flying under partial ground effect (the rotor at the right with a ground plane close to it).

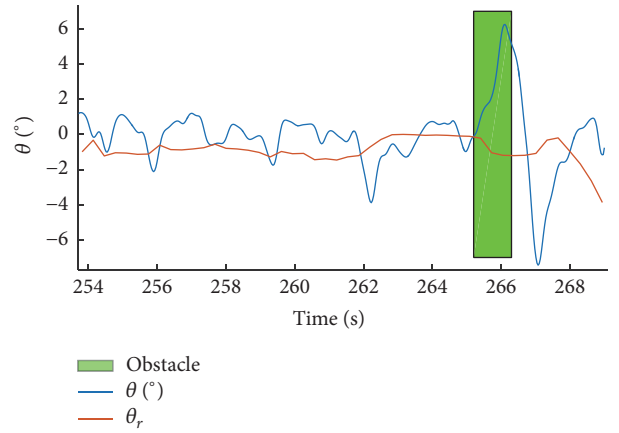

Figure 30: Partial ground effect test with the multirotor in flight.

effect for multirotors in different situations, which has been modelled similar to single-rotor helicopters in many cases in the literature. The ground effect has been shown to generate a stabilizing moment in multirotors due to the differences in height over the ground of the different rotors. Moreover, the so-called partial ground effect, when only one rotor is over the surface, has been studied. The paper has also shown by simulations and experiments which control strategies can be used to compensate this effect. In future research, the dynamic ground effect will be considered to complete these results.

Conflicts of Interest

The authors declare that they have no conflicts of interest.

Acknowledgments

This work has been supported by the AEROARMS project, funded by the European Commission under the H2020 Programme (H2020-2014-644271), the AEROMAIN (DPI2014-59383-C2-1-R) and AEROCROS (DPI2015-71524-R) projects, funded by the Spanish Ministerio de Economía, Industria y Competitividad, and the FPU Programme, funded by the Spanish Ministerio de Educación, Cultura y Deporte.

References

[1] K. P. Valavanis and G. J. Vachtsevanos, *Handbook of Unmanned Aerial Vehicles*, Springer, 2015.

[2] M. Orsag, C. Korpela, and P. Oh, "Modeling and control of MM-UAV: mobile manipulating unmanned aerial vehicle," *Journal of Intelligent and Robotic Systems: Theory and Applications*, vol. 69, no. 1-4, pp. 227–240, 2013.

[3] M. Fumagalli, R. Naldi, A. Macchelli et al., "Developing an aerial manipulator prototype: physical interaction with the environment," *IEEE Robotics and Automation Magazine*, vol. 21, no. 3, pp. 41–50, 2014.

[4] K. Kondak, A. Ollero, I. Maza et al., "Unmanned aerial systems physically interacting with the environment: load transportation, deployment, and aerial manipulation," *Handbook of Unmanned Aerial Vehicles*, pp. 2755–2785, 2015.

[5] S. Kim, H. Seo, and H. J. Kim, "Operating an unknown drawer using an aerial manipulator," in *Proceedings of the 2015 IEEE International Conference on Robotics and Automation, ICRA 2015*, pp. 5503–5508, May 2015.

[6] G. Heredia, A. E. Jimenez-Cano, I. Sanchez et al., "Control of a multirotor outdoor aerial manipulator," in *Proceedings of the 2014 IEEE/RSJ International Conference on Intelligent Robots and Systems, IROS 2014*, pp. 3417–3422, September 2014.

[7] A. E. Jimenez-Cano, J. Braga, G. Heredia, and A. Ollero, "Aerial manipulator for structure inspection by contact from the underside," in *Proceedings of the IEEE/RSJ International Conference on Intelligent Robots and Systems, IROS 2015*, pp. 1879–1884, October 2015.

[8] H. Tsukagoshi, M. Watanabe, T. Hamada, D. Ashlih, and R. Iizuka, "Aerial manipulator with perching and door-opening capability," in *Proceedings of the 2015 IEEE International Conference on Robotics and Automation, ICRA 2015*, pp. 4663–4668, May 2015.

[9] AEROARMS Project website, "Aerial Robotics Cooperative Assembly system," http://www.arcas-project.eu.

[10] ARCAS Project website, http://www.aeroarms-project.eu.

[11] I. Cheeseman and W. Bennett, "The effect of the ground on a helicopter rotor in forward flight," *ARC R&M 3021*, 1955.

[12] E. A. Fradenburgh, "The helicopter and the ground effect machine," *Journal of the American Helicopter Society*, vol. 5, no. 4, pp. 24–33, 1960.

[13] H. C. Curtiss Jr., M. Sun, W. F. Putman, and E. J. Hanker Jr., "Rotor aerodynamics in ground effect at low advance ratios," *Journal of the American Helicopter Society*, vol. 29, no. 1, pp. 48–55, 1984.

[14] T. E. Lee, J. G. Leishman, and M. Ramasamy, "Fluid dynamics of interacting blade tip vortices with a ground plane," *Journal of the American Helicopter Society*, vol. 55, no. 2, pp. 22005–2200516, 2010.

[15] P. Tanner, A. Overmeyer, L. Jenkins, C. S. Yao, and S. Bartram, "Experimental investigation of rotorcraft outwash in ground effect," in *Proceedings of the 71th Annual Forum of the American Helicopter Society*, pp. 1–26, 2015.

[16] J. S. Hayden, "Effect of the ground on helicopter hovering power required," in *Proceedings of the AHS 32nd Forum*, 1976.

[17] K. Nonaka and H. Sugizaki, "Integral sliding mode altitude control for a small model helicopter with ground effect compensation," in *Proceedings of the 2011 American Control Conference*, pp. 202–207, San Francisco, CA, June 2011.

[18] M. Bangura and R. Mahony, "Nonlinear dynamic modeling for high performance control of a quadrotor," in *Proceedings of the Australasian Conference on Robotics and Automation*, Wellington, New Zealand, 2012.

[19] D. Abeywardena, Z. Wang, G. Dissanayake, S. L. Waslander, and S. Kodagoda, "Model-aided state estimation for quadrotor micro air vehicles amidst wind disturbances," in *Proceedings of the 2014 IEEE/RSJ International Conference on Intelligent Robots and Systems, IROS 2014*, pp. 4813–4818, September 2014.

[20] M. Bangura, H. Lim, H. J. Kim, and R. Mahony, "Aerodynamic power control for multirotor aerial vehicles," in *Proceedings of the 2014 IEEE International Conference on Robotics and Automation, ICRA 2014*, pp. 529–536, June 2014.

[21] C. D. McKinnon and A. P. Schoellig, "Unscented external force and torque estimation for quadrotors," in *Proceedings of the 2016 IEEE/RSJ International Conference on Intelligent Robots and Systems, IROS 2016*, pp. 5651–5657, October 2016.

[22] T. Tomic and S. Haddadin, "A unified framework for external wrench estimation, interaction control and collision reflexes for flying robots," in *Proceedings of the 2014 IEEE/RSJ International Conference on Intelligent Robots and Systems, IROS 2014*, pp. 4197–4204, September 2014.

[23] F. Ruggiero, J. Cacace, H. Sadeghian, and V. Lippiello, "Impedance control of VToL UAVs with a momentum-based external generalized forces estimator," in *Proceedings of the 2014 IEEE International Conference on Robotics and Automation, ICRA 2014*, pp. 2093–2099, June 2014.

[24] B. Yuksel, C. Secchi, H. H. Bülthoff, and A. Franchi, "A nonlinear force observer for quadrotors and application to physical interactive tasks," in *Proceedings of the 2014 IEEE/ASME International Conference on Advanced Intelligent Mechatronics, AIM 2014*, pp. 433–440, July 2014.

[25] T. Tomic and S. Haddadin, "Simultaneous estimation of aerodynamic and contact forces in flying robots: Applications to metric wind estimation and collision detection," in *Proceedings of the 2015 IEEE International Conference on Robotics and Automation, ICRA 2015*, pp. 5290–5296, Seattle, USA, May 2015.

[26] N. Guenard, T. Hamel, and L. Eck, "Control laws for the tele operation of an unmanned aerial vehicle known as an X4-flyer," in *Proceedings of the Proceeding of the IEEE/RSJ International Conference on Intelligent Robots and Systems (IROS '06)*, pp. 3249–3254, Beijing, China, October 2006.

[27] H. Nobahari and A. R. Sharifi, "Continuous ant colony filter applied to online estimation and compensation of ground effect in automatic landing of quadrotor," *Engineering Applications of Artificial Intelligence*, vol. 32, pp. 100–111, 2014.

[28] L. Danjun, Z. Yan, S. Zongying, and L. Geng, "Autonomous landing of quadrotor based on ground effect modelling," in *Proceedings of the 34th Chinese Control Conference, CCC 2015*, pp. 5647–5652, July 2015.

[29] J. Bartholomew, A. Calway, and W. Mayol-Cuevas, "Learning to predict obstacle aerodynamics from depth images for micro air vehicles," in *Proceedings of the 2014 IEEE International Conference on Robotics and Automation, ICRA 2014*, pp. 4967–4973, June 2014.

[30] C. Hooi, F. Lagor, and D. Paley, "Flow sensing for height estimation and control of a rotor in ground effect: modeling and experimental results," in *Proceedings of the AHS 71st Annual Forum*, Virginia Beach, USA, May 2015.

[31] C. Powers, D. Mellinger, A. Kushleyev, B. Kothmann, and V. Kumar, "Influence of aerodynamics and proximity effects in quadrotor flight," in *Experimental Robotics*, vol. 88 of *Springer Tracts in Advanced Robotics*, pp. 289–302, Springer International Publishing, Heidelberg, 2013.

[32] I. Sharf, M. Nahon, A. Harmat et al., "Ground effect experiments and model validation with Draganflyer X8 rotorcraft," in *Proceedings of the 2014 International Conference on Unmanned Aircraft Systems, ICUAS 2014*, pp. 1158–1166, May 2014.

[33] D. A. Griffiths, S. Ananthan, and J. G. Leishman, "Predictions of rotor performance in ground effect using a free-vortex wake model," *Journal of the American Helicopter Society*, vol. 50, no. 4, pp. 302–314, 2005.

[34] P. Castillo, R. Lozano, and A. Dzul, *Modelling and Control of Mini-Flying Machines*, Springer, 2005.

[35] R. Mahony, V. Kumar, and P. Corke, "Multirotor aerial vehicles: modeling, estimation, and control of quadrotor," *IEEE Robotics and Automation Magazine*, vol. 19, no. 3, pp. 20–32, 2012.

[36] J. W. Seo, B. E. Lee, B. S. Kang, S. J. Oh, and K. J. Yee, "Experimental study on the small-scale rotor hover performance in

partial ground conditions," *Journal of the Korean Society for Aeronautical & Space Sciences*, vol. 38, no. 1, pp. 12–21, 2010.

[37] H. Lim, J. Park, D. Lee, and H. J. Kim, "Build your own quadrotor: Open-source projects on unmanned aerial vehicles," *IEEE Robotics and Automation Magazine*, vol. 19, no. 3, pp. 33–45, 2012.

[38] S. Bellens, J. De Schutter, and H. Bruyninckx, "A hybrid pose/ wrench control framework for quadrotor helicopters," in *Proceedings of the IEEE International Conference on Robotics and Automation (ICRA)*, 2012.